



Contents lists available at ScienceDirect



# Catalysis Today

journal homepage: [www.elsevier.com/locate/cattod](http://www.elsevier.com/locate/cattod)

## Silica-supported silver-containing OMS-2 catalysts for ethanol oxidative dehydrogenation

Valerii V. Dutov<sup>a</sup>, Grigory V. Mamontov<sup>a</sup>, Vladimir I. Sobolev<sup>a,b</sup>, Olga V. Vodyankina<sup>a,\*</sup>

<sup>a</sup> Tomsk State University, 36 Lenin Ave., Tomsk, 634050, Russia

<sup>b</sup> Boreskov Institute of Catalysis SB RAS, 5 Lavrentiev Ave., Novosibirsk, 630090, Russia

### ARTICLE INFO

#### Article history:

Received 31 December 2015

Received in revised form 14 May 2016

Accepted 20 May 2016

Available online xxx

#### Keywords:

Manganese dioxide

Octahedral molecular sieves

Ethanol

Selective oxidation

Silver

### ABSTRACT

The silver-modified cryptomelane-type crystalline and silica-supported OMS-2 catalysts (Ag/OMS-2 and Ag/OMS-2/SiO<sub>2</sub>, respectively) were prepared by impregnation, co-precipitation, and consecutive impregnation methods and tested in selective oxidation of ethanol to acetaldehyde. Modifying OMS-2 and OMS-2/SiO<sub>2</sub> catalysts by silver was shown to improve the redox properties of the catalysts and increase the ethanol oxidation rate. However, selectivity to acetaldehyde decreased with increased reaction temperature due to intensification of total oxidation on the Ag-MnO<sub>x</sub> sites. Preparation method of the catalyst affected the Ag localization and catalytic activity. Introducing silver into the OMS-2 channels provided a higher ethanol oxidation rate. The use of silica support for Ag/OMS-2 composites improved the selectivity towards acetaldehyde at higher temperatures and, therefore, increased the acetaldehyde yield in comparison with crystalline samples.

© 2016 Elsevier B.V. All rights reserved.

### 1. Introduction

Because bioethanol is one of the main potential sources for producing hydrogen and industrial chemicals such as acetaldehyde (which in turn is an intermediate in producing acetic acid, ethyl acetate, butyraldehyde, crotonaldehyde, and *n*-butanol), developing new catalysts for ethanol conversion is of importance [1]. The main advantages of gas-phase selective ethanol oxidation compared to the liquid-phase processes are the use of air as a “green” oxidant, atmospheric pressure, and simple evacuation of acetaldehyde from reaction products without time-consuming treatment of solvent. However, elevated temperatures (500–650 °C) are usually used in industrial gas-phase Ag-catalyzed selective ethanol oxidation [2]. The ethanol conversion and selectivity toward acetaldehyde are 30–70% and 90–99% per pass, respectively. The main byproduct is acetic acid, but small amounts of formic acid, ethyl acetate, CO, and CO<sub>2</sub> can also be formed.

Combining silver and other IB subgroup metals with transition metal oxides in a catalyst composition allows significantly decreasing temperature of the process while maintaining high selectivity toward acetaldehyde [3]. Earlier we showed the key role of iron additives in Si<sub>3</sub>N<sub>4</sub>-supported Ag catalysts in the efficiency of selective oxidation of ethylene glycol and ethanol to glyoxal and acetaldehyde, respectively [4,5].

Manganese oxides possessing high oxidative activity and ability to reoxidize at low temperatures are good candidates to produce effective oxidation catalysts operating under ambient conditions [6,7]. However, appropriate reaction conditions must be chosen to achieve high selectivity toward aldehyde because of the high total oxidation activity of these catalysts. For instance, gas-phase selective oxidation of ethanol to acetaldehyde over OMS-2 catalysts is commonly carried out in reaction mixtures containing low concentrations of oxygen (1–3%) [8]. Oxygen-rich mixtures (air) can be used in gas-phase selective oxidation of aliphatic alcohols with low reaction ability (such as octanol-1) and aromatic alcohols (e.g., benzyl alcohol) [7,9]. Another way to increase the selectivity is to carry out liquid-phase oxidation reactions under mild conditions [10,11].

In the present work we assume that modification of manganese oxides by silver can enhance the selectivity towards acetaldehyde while maintaining the total conversion of ethanol under ambient conditions. The use of air as an oxidant due to change in the Mn<sup>4+</sup>/Mn<sup>3+</sup> ratio in the catalyst structure is also considered.

Octahedral molecular sieve materials with a cryptomelane structure (OMS-2) attract special attention due to unique adsorptive, ion-exchanging, semi-conductive, and catalytic properties. Nanostructured materials based on cryptomelane-type manganese oxide have been extensively investigated as supercapacitors [12,13], sorbents for adsorptive desulfurization of fuel gas [14,15], H<sub>2</sub>S consumption [16], CO<sub>2</sub> capture [17], catalysts for synthesis of pharmaceutical substances [18], and valuable organic compounds [19–22]. Moreover, the OMS-2 materials are environmentally

\* Corresponding author.

E-mail address: [vodyankina.o@mail.ru](mailto:vodyankina.o@mail.ru) (O.V. Vodyankina).

friendly catalysts for selective oxidation of alcohols to corresponding aldehydes [6,7,9,23], in particular, for liquid phase alcohol oxidation [10,24].

Cryptomelane with the gross formula of  $K_xMn^{4+}_{8-x}Mn^{3+}_xO_{16}\cdot nH_2O$  is the analog of the natural mineral hollandite ( $BaMn_8O_{16}$ ), consisting of double chains of edge-sharing  $MnO_6$  octahedra linked at vertices to form  $(1 \times 1)$  and  $(2 \times 2)$  channels. The  $(2 \times 2)$  channels in the cryptomelane phase with a size of  $4.6\text{ \AA}$  are occupied by  $K^+$  ions and water molecules to stabilize the structure. The cryptomelane-type materials can be prepared via reaction between  $Mn^{2+}$  and  $MnO_4^-$  in acid solution according to both a reflux method [18,25,26] and hydrothermal synthesis [15,27]. The presence of potassium ions in the solution is an essential condition for crystallization of OMS-2 structure. Potassium cation has a suitable ionic radius compared to other monovalent ions and plays the role of a template. It can be partially substituted by other ions ( $Ag^+, Cu^{2+}, Zn^{2+}, Mg^{2+}, Co^{2+}, Ni^{2+}, NH_4^+, H^+, Na^+$ , etc.) using two main methods, namely, the ion-exchange technique (after cryptomelane phase synthesis) and the refluxing method (addition of metal salt before cryptomelane synthesis) [28].

The features of the OMS-2 materials, including their catalytic properties, depend on the nature and concentration of counter cation in the channels [29], the average oxidation state of Mn and lattice oxygen mobility [30], acid-base properties [31,32], and morphology and textural properties [33]. The average oxidation state of Mn in the OMS-2 materials may be changed from 3.4 to 3.99 due to simultaneous presence of  $Mn^{2+}$ ,  $Mn^{3+}$ , and  $Mn^{4+}$  ions in the framework [14,16,34]. The effect of temperature and pH on the manganese oxide crystallization into a cryptomelane structure was described in [35]. Amorphous manganese dioxide can only be obtained in a pH range from 5 to 7 and a temperature range of  $50\text{--}200^\circ\text{C}$ . The hollandite-type manganese oxide may be synthesized in a strongly acidic medium at  $pH = 1\text{--}2$  in a temperature range from 80 to  $120^\circ\text{C}$ .

Good catalytic performance (high TOF) of OMS-2 materials in the oxidation reactions is commonly associated with high mobility of lattice oxygen caused by a reversible  $Mn^{4+}/Mn^{3+}$  redox cycle and one-dimensional micropores adsorbing small organic molecules, as well as high surface acidity. Oxidation of organic compounds over OMS-2 catalysts follows the Mars-van Krevelen mechanism [7,36]. From this point of view, it is interesting to investigate the influence of a reoxidation rate on the catalytic activity. The effect of acid-base properties on the catalytic activity of OMS-2 catalysts in oxidation reactions, especially in selective alcohol oxidation, has not been thoroughly investigated. The effect of catalyst acidity on its catalytic properties was investigated in a liquid-phase cyclohexane oxidation to cyclohexanone and cyclohexanol for H-exchanged OMS-2 catalysts [31]. Increased acidity was shown to increase the cyclohexane conversion, while selectivity toward cyclohexanol was not changed, and selectivity toward cyclohexanone increased.

One of the ways to control the redox and acid-base properties of transition metal oxide catalysts is the use of various supports (silica, alumina, etc.). However, supported OMS-2 catalysts have not been thoroughly investigated, while other supported  $MnO_x$  catalysts are widely presented in the literature [37–40]. The alumina- and silica-supported OMS-2 catalysts were prepared and tested in total oxidation of ethanol [41] and ethyl acetate [42], respectively. To the best of our knowledge, supported OMS-2 catalysts for vapor-phase selective oxidation of alcohols are not described in the literature.

Therefore, the aim of the present research work is to design a preparation method to synthesize highly efficient supported OMS-2 catalysts for gas-phase selective oxidation of ethanol under ambient conditions (low temperature and atmospheric pressure and using air as an oxidant) and to investigate their physical-

chemical properties with special attention to surface acidity and redox properties.

## 2. Experimental

### 2.1. Sample preparation

Silver-containing OMS-2 crystalline catalysts were prepared by impregnation (Impr) and co-precipitation (CP) methods. In the impregnation method, the OMS-2 materials were primarily prepared by a hydrothermal method similar to the one described in [15,43,44]. A solution of  $KMnO_4$  (5.89 g) in distilled water (100 ml) was added gradually to an acidic solution of  $Mn(NO_3)_2\cdot 6H_2O$  (14.92 g) in distilled water (30 ml) with vigorous stirring. The obtained dark brown precipitate with mother solution was hydrothermally treated at  $120^\circ\text{C}$  for 24 h. Then the precipitate obtained was filtered, washed, and dried at  $120^\circ\text{C}$  overnight. The OMS-2 sample obtained was then impregnated with an aqueous solution of  $AgNO_3$  (0.49 M), dried overnight at  $80^\circ\text{C}$ , and calcined at  $500^\circ\text{C}$  in air. The catalyst prepared was denoted “Ag/OMS-2-Impr”. To investigate the effect of calcination temperature on the phase composition of the OMS-2, the material obtained was calcined at 300, 400, and  $500^\circ\text{C}$ . During co-precipitation,  $AgNO_3$  (0.68 g) was added to  $Mn(NO_3)_2\cdot 6H_2O$  solution with the same concentration (as for OMS-2 synthesis) before redox reaction and subsequent hydrothermal treatment (HT) under the same conditions. The precipitate obtained was calcined at  $500^\circ\text{C}$  in air. The sample was denoted “Ag/OMS-2-CP”.

Silica-supported OMS-2 catalysts were prepared by the consecutive impregnation (CI) and co-precipitation methods. A commercial mesoporous silica ( $S_{BET} = 245\text{ m}^2/\text{g}$ ,  $D_{BJH} = 9.8\text{ nm}$ ,  $V_{BJH} = 0.74\text{ cm}^3/\text{g}$ , grain sizes of 1–2 mm) was used as a support for the catalysts. Prior to introduction of active components, the silica was subjected to HT in ammonia solution at  $120^\circ\text{C}$  for 3 h, then dried at  $120^\circ\text{C}$  and calcined at  $500^\circ\text{C}$  for 5 h. Initially a  $KMnO_4/SiO_2$  sample was obtained by impregnation of silica support (8.5 g) with a solution containing  $KMnO_4$  (1.20 g) in distilled water (6.8 ml) followed by drying at  $60^\circ\text{C}$ . Then  $KMnO_4/SiO_2$  was added to acidic aqueous solution of  $Mn(NO_3)_2\cdot 6H_2O$  (3.04 g) in 30 ml of distilled water under stirring. The precipitate obtained in the mother solution was placed in a Teflon autoclave and exposed at  $120^\circ\text{C}$  for 24 h. Then the precipitate was filtered, washed with distilled water, and dried at  $120^\circ\text{C}$ . The OMS-2/ $SiO_2$  sample obtained was impregnated with aqueous solution of  $AgNO_3$  (0.69 M), dried overnight at  $80^\circ\text{C}$ , and calcined at  $500^\circ\text{C}$  in air. The catalyst prepared was denoted “Ag/OMS-2/ $SiO_2$ -CI”.

In the co-precipitation method,  $KMnO_4/SiO_2$  was added under stirring to an acidic aqueous solution containing the same amount of  $Mn(NO_3)_2\cdot 6H_2O$  and 0.787 g of  $AgNO_3$ . The precipitate obtained was hydrothermally treated in mother solution under the same conditions, dried, and calcined at  $500^\circ\text{C}$  in air. The catalyst prepared was denoted “Ag/OMS-2/ $SiO_2$ -CP”. The Ag/ $SiO_2$  catalyst was prepared by impregnation of silica support with aqueous solution of  $AgNO_3$  (0.63 M) followed by drying at  $80^\circ\text{C}$  and calcination in air at  $500^\circ\text{C}$ . Theoretical silver loading in all prepared catalysts was 5 wt%.

### 2.2. Sample characterization

The catalysts prepared were examined by  $N_2$  adsorption at  $-196^\circ\text{C}$ , atomic emission spectroscopy (AES ICP), powder X-ray diffraction (XRD), temperature-programmed reduction (TPR), temperature-programmed oxidation (TPO), temperature-programmed surface reaction of adsorbed ethanol (TPSR- $C_2H_5OH$ ),

NH<sub>3</sub> pulse adsorption, thermogravimetric analysis, and differential scanning calorimetry coupled with mass spectrometry (TGA-DSC-MS).

The surface area and pore diameter of the samples were measured by nitrogen sorption at -196 °C using the TriStar II 3020 analyzer (Micromeritics, USA). Prior to experiments, all samples were outgassed (10<sup>-2</sup> Torr) at 200 °C for 2 h. The specific surface area was determined by the BET method. The pore size distribution was calculated from the desorption branch of the adsorption-desorption isotherm according to the Barrett-Joyner-Halenda (BJH) method. Micropore area was calculated by means of the MP method.

Chemical composition of the samples was analyzed using the 4100 MP-AES EuroEA 3000 analyzer (Agilent Technologies, USA). The OMS-2 samples were dissolved in a concentrated HNO<sub>3</sub> in the presence of sulphite-anion. Silica-supported OMS-2/SiO<sub>2</sub> catalysts were dissolved in the same mixture, but with the addition of HF.

X-ray diffraction (XRD) patterns were recorded on the MiniFlex 600 (Rigaku, Japan) diffractometer using monochromatized Cu-K $\alpha$  radiation ( $\lambda = 1.5418 \text{ \AA}$ ) with a power setting of 40 kV and 15 mA. The XRD patterns were recorded in the range of  $2\theta = 10\text{--}90^\circ$  with a scanning rate of 2°/min. The phase identification was made according to the PCPDFWIN database.

The redox properties of catalysts were investigated by TPR and TPO using the AutoChem HP chemisorption analyzer (Micromeritics, USA) equipped with a thermal conductivity detector (TCD). The TPR experiments were performed in a temperature range from room temperature to 700 °C at a heating rate of 10 °C/min using a 10 vol%H<sub>2</sub>/Ar mixture (flow rate of 20 ml/min). The TPO experiments were performed in the temperature range from room temperature to 500 °C at a heating rate of 10 °C/min using a 5 vol%O<sub>2</sub>/He mixture (flow rate of 20 ml/min). Before TPO experiments the samples were reduced in a TPR regime to 500 °C.

To investigate the interaction of C<sub>2</sub>H<sub>5</sub>OH molecule with the catalyst surface TPSR-C<sub>2</sub>H<sub>5</sub>OH, experiments were performed using the AutoChem HP chemisorption analyzer coupled with the UGA 300 quadrupole mass spectrometer (Stanford Research Systems, USA). Prior to experiments the catalyst samples were heated to 400 °C in a 5 vol%O<sub>2</sub>/He mixture. Then ethanol was adsorbed at 80 °C in a pulse mode using syringe (each impulse volume was 1  $\mu\text{l}$ ). Doses of ethanol were injected into Ar flow (30 ml/min) until peak areas became identical. Ethanol desorption was performed in the temperature range 80–600 °C with a heating rate of 10 °C/min in Ar flow (30 ml/min).

Pulse experiments using the AutoChem HP analyzer were performed to evaluate the number of acid sites on the surface of catalysts NH<sub>3</sub>. Prior to the experiments the catalysts were heated in He to up to 400 °C. Then NH<sub>3</sub> adsorption was performed at 100 °C in a He flow (30 ml/min) injecting 10 vol%NH<sub>3</sub>/He mixture via loop with  $V = 1 \text{ cm}^3$ . The total amount of adsorbed NH<sub>3</sub> was calculated from peak areas using a calibration coefficient.

The TG-DSC-MS analysis of the samples was performed using the STA 449 F1 Jupiter analyzer (Netzsch, Germany) coupled with the quadrupole mass spectrometer QMS 403D Aélos (Netzsch, Germany). The samples (5–10 mg) were placed in an Al<sub>2</sub>O<sub>3</sub> crucible and heated from 25 to 800 °C at the rate of 10 °C/min in Ar atmosphere (70 ml/min) and Ar/air atmosphere (20 ml/min Ar + 50 ml/min air).

### 2.3. Catalytic test

Catalytic activity of the samples in the ethanol oxidation was tested in a flow fixed-bed reactor at atmospheric pressure using 0.5 g of catalyst according to the procedure described in [45]. Gas mixture containing 2 vol%C<sub>2</sub>H<sub>5</sub>OH and 18 vol%O<sub>2</sub> in He was passed through the reactor at a total flow rate of 60 cm<sup>3</sup>/min. The effluents

**Table 1**  
Textural properties of the prepared catalysts.

Catalyst	$S_{sp}, \text{m}^2/\text{g}^a$	$D_p, \text{nm}^b$	$V_p, \text{cm}^3/\text{g}^c$	$S_{micro}, \text{m}^2/\text{g}^d$	$d_{MnO_2}, \text{nm}^e$
OMS-2	29.5	15.7	0.14	19.5	19.5
Ag/OMS-2-Impr	27.0	17.0	0.12	12.9	19.0
Ag/OMS-2-CP	37.6	13.7	0.14	18.7	17.4
OMS-2/SiO <sub>2</sub>	160.5	14.8	0.68	21.8	13.9
Ag/OMS-2/SiO <sub>2</sub> -Cl	154.6	15.1	0.67	17.6	14.1
Ag/OMS-2/SiO <sub>2</sub> -CP	150.4	15.4	0.67	22.8	14.3
Ag/SiO <sub>2</sub>	148	15.3	0.67	15.0	—
SiO <sub>2</sub>	177.3	13.4	0.70	26.8	—

<sup>a</sup> Specific surface area calculated by applying the BET method.

<sup>b</sup> Average pore diameter calculated from BJH method as  $4V_p/S_{ext}$ .

<sup>c</sup> Total pore volume.

<sup>d</sup> Surface area of micropores calculated by applying the MP method.

<sup>e</sup> Crystallite size calculated using Scherrer's equation.

from the reactor were analyzed by an online gas chromatograph. The catalysts were treated in 8 vol%O<sub>2</sub>/He at 500 °C for 1 h before the catalytic experiments.

## 3. Results and discussion

### 3.1. Textural properties of the samples

N<sub>2</sub> adsorption-desorption isotherms for crystalline (namely, OMS-2 support, Ag/OMS-2-Impr, and Ag/OMS-2-CP catalysts) and supported (OMS-2/SiO<sub>2</sub>, Ag/OMS-2/SiO<sub>2</sub>-Cl, and Ag/OMS-2/SiO<sub>2</sub>-CP) samples are shown in Fig. 1(a, b). It is clearly seen that the isotherms for both series of samples may be attributed to IV type isotherm with H1 hysteresis loop according to IUPAC classification. Table 1 shows textural properties of the catalysts. One can see that the average pore diameter for crystalline and supported catalysts differs insignificantly; however, the porous structure of these catalysts is different. The specific surface area of crystalline and supported samples is ~30 and ~150 m<sup>2</sup>/g, respectively. The surface of crystalline OMS-2 materials consists of a micropore surface area (from 48 to 66% of the total area) and the external surface of the crystallites. The micropore area for the Ag/OMS-2-Impr catalyst is less than that of OMS-2 and Ag/OMS-2-CP. The decreased micropore area indicates partial blocking of porous structure by silver or silver oxide particles when the samples were prepared by the wetness impregnation method. In the samples synthesized by the CP method, silver ions substitute the potassium ions in the channels of OMS-2 without blocking the porous structure. Surface area for the Ag/OMS-2-CP catalyst is higher compared to OMS-2 and Ag/OMS-2-Impr, which is associated with smaller crystallite sizes (according to the XRD data).

The porosity of supported OMS-2 catalysts includes the mesoporous structure of silica support and microporous structure of the supported OMS-2 phase. Reduction of surface area for supported OMS-2/SiO<sub>2</sub>, Ag/OMS-2/SiO<sub>2</sub>-Cl, and OMS-2/SiO<sub>2</sub>-CP catalysts in comparison with the initial silica support has resulted from distribution of active components (manganese oxide and silver) inside the pores of silica. Micropore areas are similar for SiO<sub>2</sub>, supported OMS-2/SiO<sub>2</sub>, Ag/OMS-2/SiO<sub>2</sub>-Cl, and Ag/OMS-2/SiO<sub>2</sub>-CP catalysts. During the OMS-2 introduction onto silica support, the initial micropores of silica were blocked, while new micropores appeared due to formation of the OMS-2 structure.

### 3.2. Phase and chemical composition

The XRD patterns for OMS-2 samples calcined at different temperatures are presented in Fig. 2. One can see that the as-prepared OMS-2 sample (dried at 120 °C) contains cryptomelane KMn<sub>8</sub>O<sub>16</sub>, pyrolusite ( $\beta$ -MnO<sub>2</sub>), and nsutite  $\gamma$ -Mn(O,OH)<sub>2</sub> phases. The main reflections at  $2\theta = 12.7, 18.0, 28.6, 37.4, 49.9$ , and 60.2°

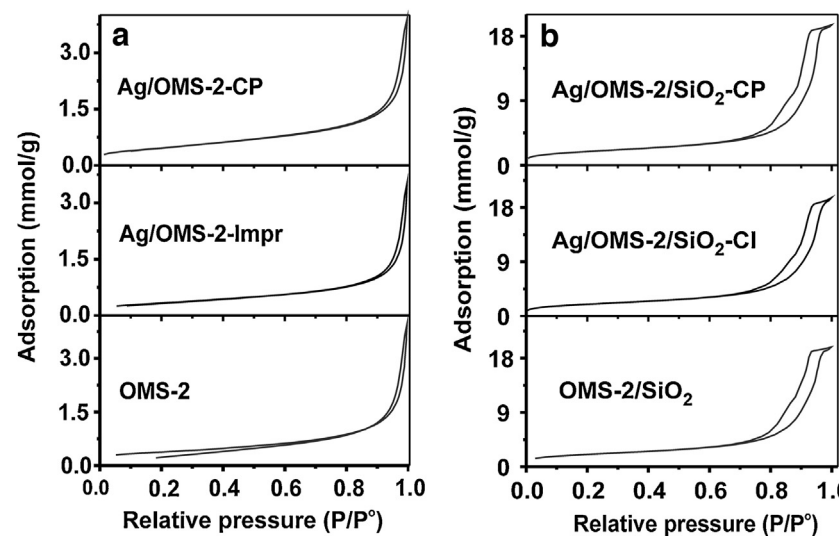


**Fig. 1.** The N<sub>2</sub> adsorption-desorption isotherms for crystalline (a) and silica-supported (b) OMS-2 catalysts.

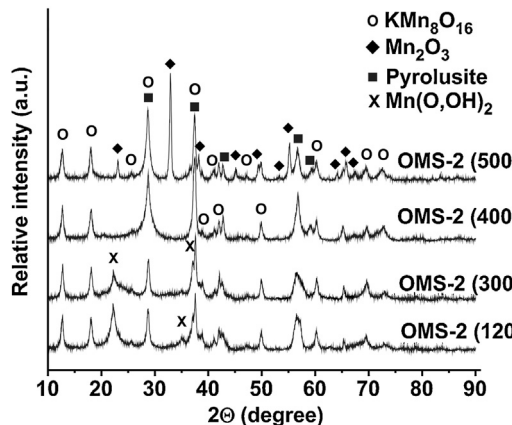


**Fig. 2.** Influence of calcination temperature on the phase composition of OMS-2 sample.

are attributed to the (110), (200), (310), (211), (411), and (521) planes of cryptomelane, respectively [43,46,47]. Reflections from the pyrolusite phase at  $2\theta=28.6$  and  $37.4^\circ$  are similar to those of cryptomelane, therefore, the presence of a pyrolusite phase is difficult to prove unambiguously. However, additional reflections with low intensity at  $2\theta=42.7$ ,  $56.6$ , and  $59.3^\circ$  may correspond to the (111), (211), and (220) planes of a pyrolusite phase, respectively. Reflections at  $2\theta=37.1$  and  $22.2^\circ$  may be attributed to the (220) and (101) planes of nsutite. The nsutite and pyrolusite phases may be formed in the course of the HT as impurity phases [6,48].

The increase of calcination temperature to  $400^\circ\text{C}$  results in disappearance of nsutite reflections accompanied by increase of reflection intensity for cryptomelane and pyrolusite phases caused by dehydration. Increase of the calcination temperature to  $500^\circ\text{C}$  leads to partial decomposition of manganese dioxide (pyrolusite) and OMS-2 with formation of a bixbyite phase (Mn<sub>2</sub>O<sub>3</sub>). Reflections at  $2\theta=23.0$ ,  $32.9$ ,  $38.2$ ,  $55.2$ , and  $65.8^\circ$  can be attributed to the (211), (222), (400), (440), and (622) planes of Mn<sub>2</sub>O<sub>3</sub>, respectively.

Fig. 3 shows the XRD patterns for Ag/OMS-2-Impr, Ag/OMS-2-CP, and OMS-2 catalysts calcined at  $500^\circ\text{C}$ . The phases of cryptomelane, pyrolusite, and bixbyite were observed for all samples. It is clearly seen that intensity of the diffraction peak at  $2\theta=32.9^\circ$ , attributed to the Mn<sub>2</sub>O<sub>3</sub> phase, is much lower for Ag-containing samples (Ag/OMS-2-Impr and Ag/OMS-2-CP) in

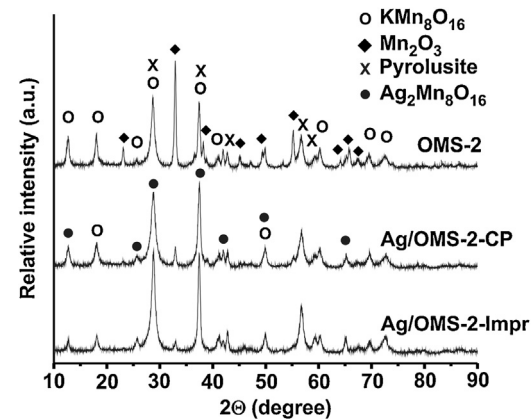


**Fig. 3.** XRD patterns for OMS-2, Ag/OMS-2-Impr and Ag/OMS-2-CP catalysts calcined at  $500^\circ\text{C}$ .

comparison with the peak for the OMS-2. Reduction of Mn<sub>2</sub>O<sub>3</sub> content in silver-containing catalysts may be associated with increase of thermal stability of the sample due to incorporation of silver ions in the channels of OMS-2 forming an Ag<sub>2</sub>Mn<sub>8</sub>O<sub>16</sub> phase. No visible diffraction peaks for silver-containing phases (metallic Ag or Ag<sub>2</sub>O) are observed for Ag/OMS-2-Impr and Ag/OMS-2-CP catalysts, which is associated with a highly dispersed Ag state. Similar results were obtained in [46,49]. In the Ag/OMS-2-CP catalyst formation of silver-substituted cryptomelane phase, Ag<sub>2</sub>Mn<sub>8</sub>O<sub>16</sub> occurs via partial substitution of potassium in the channels of OMS-2. However, this cannot be proved by means of XRD due to the similarity of cryptomelane and Ag<sub>2</sub>Mn<sub>8</sub>O<sub>16</sub> structures. Formation of an Ag<sub>2</sub>Mn<sub>8</sub>O<sub>16</sub> phase in the Ag/OMS-2-Impr sample is also possible. Silver ions are able to substitute water molecules in the channels of the OMS-2 and occupy the vacant sites inaccessible for potassium cations because potassium cations have a slightly larger ionic radius (0.24 and 0.28 nm for Ag<sup>+</sup> and K<sup>+</sup>, respectively) [50]. A similar problem about identification of an Ag<sub>2</sub>Mn<sub>8</sub>O<sub>16</sub> phase in the presence of MnO<sub>2</sub> was mentioned in [51]. Here we attempted to prove the presence of an Ag<sub>2</sub>Mn<sub>8</sub>O<sub>16</sub> phase using thermal analysis data.

Thermal stability of the samples was investigated by the TGA-DSC-MS. Fig. 4 (a, b) shows thermal analysis data obtained for OMS-2, Ag/OMS-2-Impr, and Ag/OMS-2-CP catalysts in inert and oxygen-containing atmospheres. Decomposition of pyrolusite,

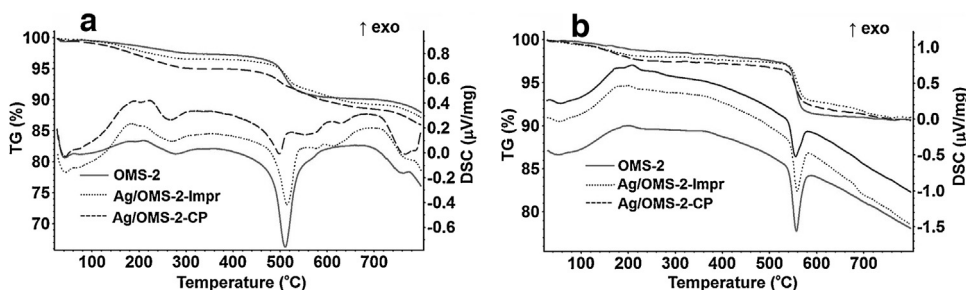


**Fig. 4.** TG-DSC data for as-prepared (dried) OMS-2, Ag/OMS-2-Impr and Ag/OMS-2-CP catalysts in Ar (a) and Ar/air (b) atmospheres.

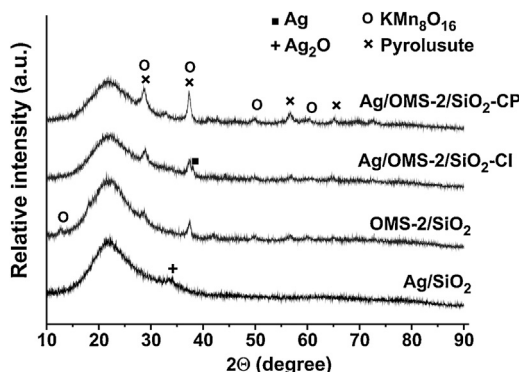
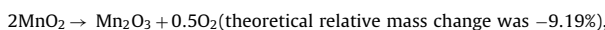


**Fig. 5.** XRD patterns for Ag/SiO<sub>2</sub>, OMS-2/SiO<sub>2</sub>, Ag/OMS-2/SiO<sub>2</sub>-Cl, Ag/OMS-2/SiO<sub>2</sub>-CP catalysts calcined at 500°C.

cryptomelane, and Ag<sub>2</sub>Mn<sub>8</sub>O<sub>16</sub> was assumed to occur according to the following reactions:



One can see that for all samples, TG curves obtained in Ar atmosphere are characterized by two stages of weight loss. According to MS data (not shown) the first stage of weight loss in the temperature range from 25 to 360°C is connected with decomposition of HNO<sub>3</sub> residuals (peak of NO at 160°C), desorption of CO<sub>2</sub> (peak at 200°C), and water (peak at 270°C). The second stage of weight loss in the range from 360 to 680°C is associated with decomposition of OMS-2, MnO<sub>2</sub>, and Ag<sub>2</sub>Mn<sub>8</sub>O<sub>16</sub> phases to form Mn<sub>2</sub>O<sub>3</sub>. The weight loss is 7.13% for OMS-2 and Ag/OMS-2 samples and 6.37% for Ag/OMS-2-CP catalyst. The area (enthalpy) of peak at 500–520°C corresponding to OMS-2 (MnO<sub>2</sub>) → Mn<sub>2</sub>O<sub>3</sub> phase transition decreases in the order OMS-2 > Ag/OMS-2-Impr > Ag/OMS-2-CP. One can see that weight loss for silver-containing catalysts occurs more slowly and in a wider temperature range than for OMS-2 catalysts. Moreover, additional high-temperature wide endothermic peaks and a corresponding O<sub>2</sub> desorption peak on the mass spectra are observed. Thus, the quantity of cryptomelane and/or MnO<sub>2</sub> phases in the Ag-containing catalysts decreases due to formation of the Ag<sub>2</sub>Mn<sub>8</sub>O<sub>16</sub> phase. This phase is characterized by higher thermal stability than MnO<sub>2</sub> and KMn<sub>8</sub>O<sub>16</sub>. The content of the Ag<sub>2</sub>Mn<sub>8</sub>O<sub>16</sub> phase is higher for the Ag/OMS-2-CP catalyst than for the Ag/OMS-2-Impr sample. TG-DSC data obtained in oxygen-containing atmosphere (see Fig. 4b) is similar to that obtained in Ar flow.

Fig. 5 shows the XRD patterns for Ag/SiO<sub>2</sub> and supported OMS-2/SiO<sub>2</sub>, Ag/OMS-2/SiO<sub>2</sub>-Cl, and Ag/OMS-2/SiO<sub>2</sub>-CP catalysts calcined at 500°C. A wide diffraction peak with low intensity at

$2\theta = 33^\circ$  was observed for the Ag/SiO<sub>2</sub> sample. This peak may be attributed to highly dispersed Ag<sub>2</sub>O [52]. Pyrolusite and cryptomelane phases are observed for all Mn-containing samples. However, characteristic reflexes of the OMS-2 phase at  $2\theta = 12.7$  and  $18.0^\circ$  cannot be detected because of the wide halo of amorphous silica and low amount of manganese in the catalysts. No visible diffraction peaks of Mn<sub>2</sub>O<sub>3</sub> are observed, probably due to low Mn content. Weak reflection from metallic silver at  $2\theta = 38.0^\circ$  is observed only for the Ag/OMS-2/SiO<sub>2</sub>-Cl catalyst. The absence of any diffraction peaks of the metallic silver for Ag/OMS-2/SiO<sub>2</sub>-CP is connected with low loading of silver in this sample (see Table 2) as well as Ag incorporation in the OMS-2 structure.

Table 2 shows the chemical composition of the prepared crystalline and supported OMS-2 catalysts. One can see that silver loading in the catalysts prepared by the CP method is lower than the theoretical amount. The decrease of silver in the catalysts prepared by the CP method may be associated with leaching of silver during the HT. Loading of potassium in the Ag/OMS-2-Impr and Ag/OMS-2-CP catalysts is less than that in OMS-2 due to partial substitution of potassium ions in the channels of the OMS-2. Silver occupies the (0 0 1/2) positions in the OMS-2 channels, while potassium occupies (0 0 0) positions [49]. Therefore, an additional silver atom per unit cell appears during the potassium substitution. When silver is introduced into the OMS-2 structure, additional Mn<sup>3+</sup> ions appear to maintain the charge balance, and oxygen vacancies are formed in the framework, playing a crucial role in diffusion of lattice oxygen.

Acid-base and redox properties of the catalyst surface play a crucial role in alcohol oxidation reactions. Alcohol molecules as Lewis bases are adsorbed on the Lewis acid sites of the catalyst forming ethoxide species. According to data in the literature, the OMS-2 catalysts are characterized by strong Lewis acidity and weak Brønsted acid sites [32,53]. Basic properties of the OMS-2 catalysts are poor, which is confirmed by our CO<sub>2</sub> adsorption data. No detectable adsorption of CO<sub>2</sub> is observed in a pulse adsorption experiment at 100°C. To investigate the acid properties of the samples prepared, the NH<sub>3</sub> pulse adsorption experiments were carried out. Table 2 shows the number of acid sites per gram of the catalyst and those normalized on the surface area of the samples. One can see that for Ag/OMS-2-Impr, the concentration of the acid sites per gram of the sample (or per nm<sup>2</sup> of the surface area) is much lower than that for OMS-2 and Ag/OMS-2-CP. This may be associated with a partial blocking of porous structure and acid sites by silver-containing species. The number of acid sites per nm<sup>2</sup> for the Ag/OMS-2-CP sample was slightly lower compared to the number for the OMS-2 sample. This may be associated with the changing of the Mn<sup>4+</sup>/Mn<sup>3+</sup> ratio in the presence of silver. Supported OMS-2/SiO<sub>2</sub>, Ag/OMS-2/SiO<sub>2</sub>-Cl, and Ag/OMS-2/SiO<sub>2</sub>-CP samples have much lower acidity than the crystalline catalysts. It is clearly seen that the number of acid sites is similar for all supported catalysts. Thus, the use of silica as a support results in reducing the density of acid sites and equalizing the acidity for the samples prepared by different methods.

**Table 2**

Chemical composition and acid properties of the prepared catalysts.

Catalyst	Mn, wt.%	K, wt.%	Ag, wt.%	Ag/Mn molar ratio	Acidity, $\mu\text{mol-NH}_3/\text{g}$	Acidity, $\text{N}/\text{nm}^2$
OMS-2	58.9	3.20	–	–	112	2.3
Ag/OMS-2-Impr	56.5	2.30	5.00	0.045	30	0.68
Ag/OMS-2-CP	56.8	2.40	3.70	0.033	132	2.11
OMS-2/SiO <sub>2</sub>	3.4	0.17	–	–	25	0.09
Ag/OMS-2/SiO <sub>2</sub> -Cl	3.3	0.16	5.39	0.832	30	0.12
Ag/OMS-2/SiO <sub>2</sub> -CP	7.2	0.09	0.95	0.067	29	0.11

Thus, from the data presented, one can conclude that the method used to prepare the crystalline catalysts influences the localization of silver. In samples prepared by CP, silver ions are predominantly located in the channels of the OMS-2 and partly substitute the K<sup>+</sup> due to similar ionic radius. However, the existence of highly dispersed silver species on the external surface of the OMS-2 cannot be excluded. In samples prepared by Impr, silver predominantly forms highly dispersed species (clusters) on the external surface of the crystallites. However, the introduction of silver in the OMS-2 framework is also possible.

### 3.3. Characterization of active surface and catalytic properties

The ratio between reduction and reoxidation of the catalyst surface influences the selectivity of the process of oxidation reaction. From this point of view, it is interesting to study the reducing and reoxidation abilities of the catalysts. Fig. 6(a, b) shows the TPR profiles for crystalline (a) and supported (b) catalysts. The reduction of manganese dioxide is a multistep process [30]. For the OMS-2 sample, two peaks of hydrogen consumption are observed. The first peak at 316 °C may be associated with reduction of MnO<sub>2</sub> to form Mn<sub>3</sub>O<sub>4</sub>, while the second peak at 358 °C corresponds to reduction of Mn<sub>3</sub>O<sub>4</sub> into MnO [54]. Three overlapping peaks at lower temperature are observed for Ag-containing samples. Peaks at 195, 227, and 265 °C for Ag/OMS-2-Impr sample and peaks at 227, 250, and 281 °C for Ag/OMS-2-CP may be attributed to consecutive reduction of manganese oxides strongly interacting with silver. The decrease of reduction temperature of MnO<sub>x</sub> in the presence of silver is commonly attributed to spillover of hydrogen from silver clusters to manganese oxide [55]. However, silver is characterized by weak adsorption of hydrogen [56]. Therefore, the decrease in reduction temperature is probably connected with oxygen spillover from the Mn oxide surface to silver clusters.

In silica-supported OMS-2/SiO<sub>2</sub> catalyst, a one-step reduction occurs at 320 °C due to higher dispersion of MnO<sub>2</sub>. Addition of silver results in the decrease in reduction temperature of manganese dioxide and the appearance of several overlapping peaks. High temperature peaks at 176, 219, and 287 °C for Ag/OMS-2/SiO<sub>2</sub>-Cl and peaks at 160, 239, and 305 °C for the Ag/OMS-2/SiO<sub>2</sub>-CP catalyst may be attributed to a multistep reduction of manganese dioxide interacting with silver. Low-temperature H<sub>2</sub> consumption peaks at 50 and 92 °C connected with reduction of AgO<sub>x</sub> species on the silica surface [57,58] are observed only for the Ag/SiO<sub>2</sub> and Ag/OMS-2/SiO<sub>2</sub>-Cl catalysts. Thus, according to the TPR and XRD data, one can conclude that the method to prepare the supported catalyst also impacts the localization of silver. In sample prepared by co-precipitation, silver interacts only with manganese oxide and is located in the OMS-2 framework. Interaction of silver ions with silica surface is poor, especially at low pH, due to low charge density of the silica surface [59]. Therefore, silver is removed (leached) from the silica surface in the course of the HT of the Ag/OMS-2/SiO<sub>2</sub>-CP catalyst. In sample prepared by consecutive impregnation, silver-containing species interact with manganese dioxide and silica surface, which is confirmed by TPR data.

To sum up, adding silver facilitates the reduction of manganese oxides in both crystalline and supported samples due to strong

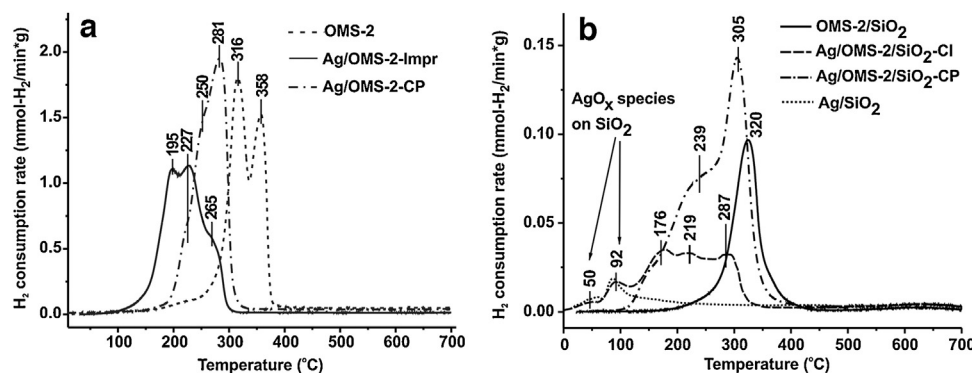
interaction of silver with manganese oxide [58]. Silver may interact with the OMS-2 phase by means of the interface between AgO<sub>x</sub> species and manganese oxide. Ag ions may be introduced into the channels of the OMS-2, providing formation of Mn<sup>3+</sup> and oxygen vacancies in the framework, which are crucial for lattice oxygen diffusion. Application of different preparation methods allows controlling the character of the silver-manganese oxide interaction and catalytic properties of the catalysts.

According to the Mars-van Krevelen concept, both reoxidation of the catalyst surface and restoration of lattice oxygen are of importance for oxidation reactions over oxide catalysts. Obviously, for total oxidation reactions high oxygen coverage of the catalyst surface is required and provided by the high reoxidation rate of the catalyst surface. We attempted to investigate the reoxidation of the prepared catalysts under model conditions (TPO regime). Fig. 7(a, b) shows the TPO profiles for crystalline (a) and supported samples (b). One can see that reoxidation of crystalline catalysts occurs via two steps. Two overlapping peaks at 330 and 470 °C are observed for the OMS-2 and Ag/OMS-2-Impr catalysts, while for Ag/OMS-2-CP samples the reoxidation occurs at 330 and 400 °C. Decreased reoxidation temperature may be associated with stronger interaction of silver with manganese oxides in the Ag/OMS-2-CP catalyst compared to Ag/OMS-2-Impr. However, no visible difference in the reoxidation rates for crystalline catalysts was observed in the temperature range from room temperature to 250 °C.

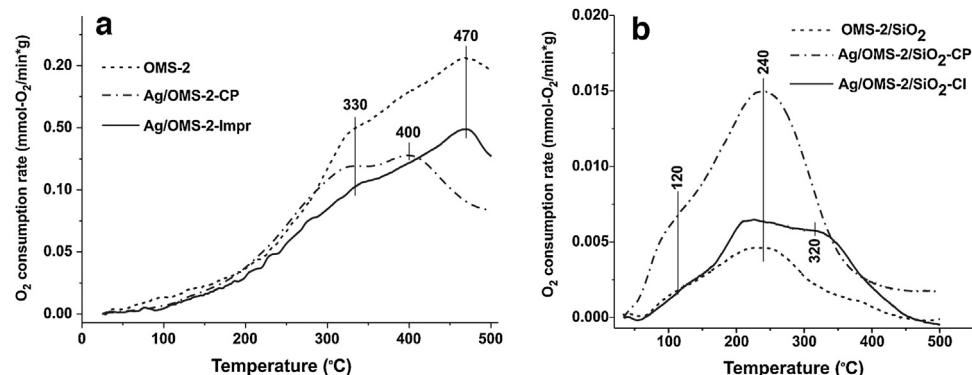
A multistep reoxidation is observed for supported OMS-2 catalysts at lower temperatures than for crystalline samples. This is caused by higher dispersion of Mn oxide particles. The maximum rate of reoxidation is observed at 220–240 °C for all supported catalysts. However, the reoxidation rate for the Ag/OMS-2/SiO<sub>2</sub>-Cl samples is higher than the rate for the OMS-2/SiO<sub>2</sub>. Thus, silver may facilitate the reoxidation of manganese oxides. The higher reoxidation rate for Ag/OMS-2/SiO<sub>2</sub>-CP catalyst than for Ag/OMS-2/SiO<sub>2</sub>-Cl may be associated with the higher amount of manganese in the catalyst.

The TPSR-C<sub>2</sub>H<sub>5</sub>OH experiments were performed to investigate the interaction of an ethanol molecule with the catalyst surface. Fig. 8(a, b) shows the desorption curves of products formed during the TPSR of adsorbed ethanol over crystalline catalysts. Two CO<sub>2</sub> evolution peaks at 175 and 230 °C (Fig. 8a) assigned to different adsorption-reaction sites and two H<sub>2</sub>O desorption peaks at 136 and 281 °C (Fig. 8b) are observed for all catalysts. A similar desorption profile consisting of two peaks of CO<sub>2</sub> was observed in [30,41]. No other products, and in particular, no acetaldehyde and acetic acid, are observed. The TPSR data correlate with the catalytic properties. Increased CO<sub>2</sub> yield is observed for crystalline catalysts in a temperature range from 170 to 230 °C.

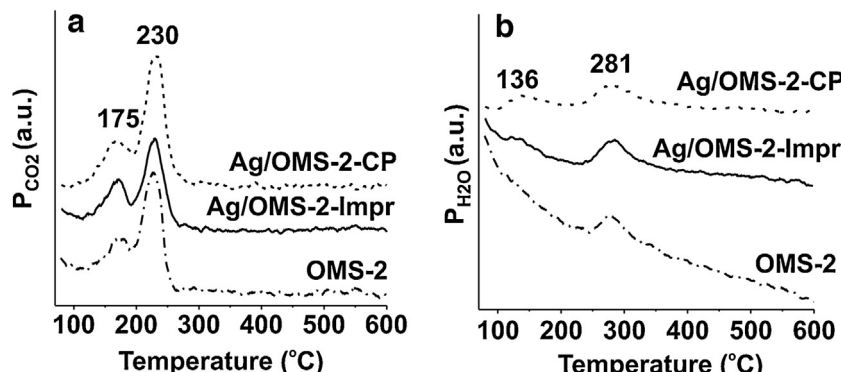
The activity of the prepared catalysts in a selective ethanol oxidation was examined by means of temperature-programmed reaction under atmospheric pressure. Fig. 9 shows the temperature dependence of ethanol conversion (Fig. 9a), selectivity toward acetaldehyde (Fig. 9b), and selectivity toward CO<sub>x</sub> (Fig. 9c) for crystalline catalyst. Acetaldehyde and CO<sub>2</sub> are the main reaction products and no other products, for example ethylene, acetic acid, or ethyl acetate, are observed. The OMS-2, Ag/OMS-2-Impr, and Ag/OMS-2-CP samples have high selectivity toward acetaldehyde



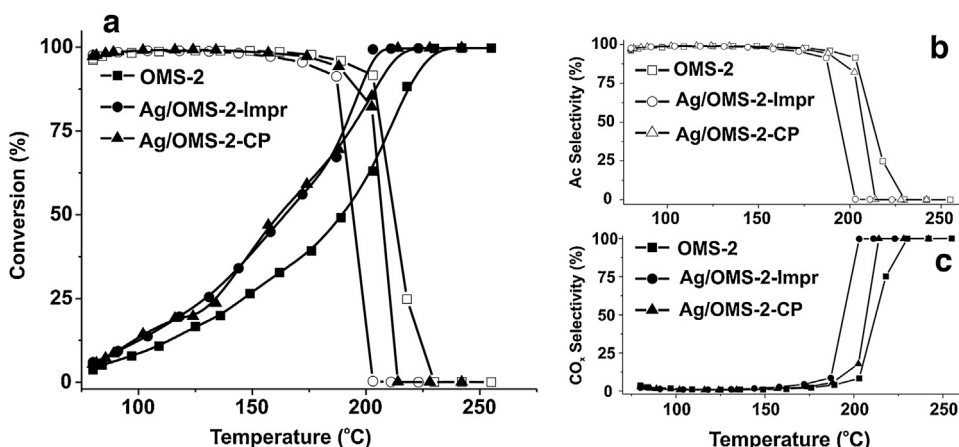
**Fig. 6.** TPR-H<sub>2</sub> profiles for crystalline OMS-2, Ag/OMS-2-Impr, Ag/OMS-2-CP (a) and supported Ag/SiO<sub>2</sub>, OMS-2/SiO<sub>2</sub>, Ag/OMS-2/SiO<sub>2</sub>-CP, Ag/OMS-2/SiO<sub>2</sub>-Cl (b) catalysts.



**Fig. 7.** TPO profiles for crystalline OMS-2, Ag/OMS-2-Impr, Ag/OMS-2-CP (a) and supported OMS-2/SiO<sub>2</sub>, Ag/OMS-2/SiO<sub>2</sub>-CP, Ag/OMS-2/SiO<sub>2</sub>-Cl (b) catalysts.



**Fig. 8.** Desorption curves of CO<sub>2</sub> (a) and H<sub>2</sub>O (b) formed during TPSR of adsorbed ethanol for crystalline OMS-2, Ag/OMS-2-Impr and Ag/OMS-2-CP catalysts.

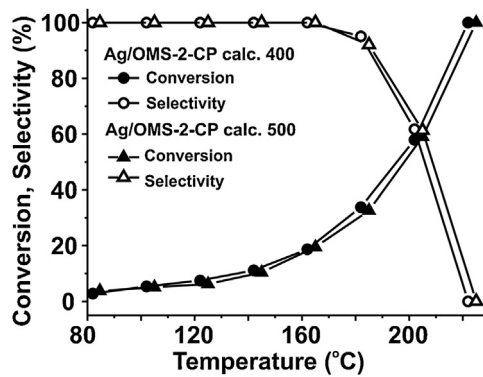


**Fig. 9.** Temperature dependences of ethanol conversion (a), selectivity toward acetaldehyde (b) and CO<sub>x</sub> (c) for crystalline catalysts (Reaction conditions: m = 0.5 g, GHSV = 7200 ml g<sup>-1</sup> H<sup>-1</sup>, Et/O<sub>2</sub> = 1/9).

**Table 3**

Comparison of various Ag-containing catalysts from the literature and the present work for gas-phase ethanol oxidation.

Catalyst	Ag, wt. %	Activity*10 <sup>-2</sup> , mol-Et/g-kat*h	TOF <sup>a</sup> , h <sup>-1</sup>	Reaction conditions			S <sub>Ac</sub> , %	STY <sup>b</sup> , h <sup>-1</sup>	Reference
				GHSV, ml/g*h	T, °C	Et/O <sub>2</sub> <sup>c</sup>			
Ag/OMS-2	–	1.25	–	36000	190	1/2	98	–	[6]
Ag/OMS-2	–	5.52	–	36000	230	1/2	95	26	[62]
Nanoporous Ag	100	46.3	50	133333	250	2/1	95	21	[60]
Ag/Fe-Si <sub>3</sub> N <sub>4</sub>	4.9	0.58	12.7	7200	283	1/9	96	4.9	[45]
Ag/MgCuCr <sub>2</sub> O <sub>4</sub>	0.89	1.23	149.2	100000	225	1/3	99	65	[61]
OMS-2	–	0.43	–	7200	170	1/9	98	–	This work
Ag/OMS-2-CP	3.7	0.66	19.3	7200	170	1/9	97	7.7	This work
Ag/OMS-2-Impr	5	0.64	13.8	7200	170	1/9	96	5.3	This work
Ag/OMS-2-CP	3.7	1.41	41.3	36000	200	1/9	58	9.8	This work
Ag/OMS-2/SiO <sub>2</sub> -CP	0.95	1.91	217.6	36000	230	1/9	85	75.4	This work
OMS-2/SiO <sub>2</sub>	–	0.15	–	7200	170	1/9	98	–	This work
Ag/OMS-2/SiO <sub>2</sub> -Cl	5.39	0.23	4.6	7200	170	1/9	98	1.81	This work
Ag/OMS-2/SiO <sub>2</sub> -CP	0.95	0.28	32.1	7200	170	1/9	98	12.8	This work

<sup>a</sup> TOF calculated as amount of ethanol (in mol) converted per mol of silver in the catalyst per hour (mol-Et\*mol<sup>-1</sup>Ag\*h<sup>-1</sup>).<sup>b</sup> Space-time-yield in galdehyde \*g<sup>-1</sup>silver \*h<sup>-1</sup>.<sup>c</sup> Molar ratio of ethanol to oxygen in the reaction mixture.**Fig. 10.** Temperature dependences of ethanol conversion and selectivity toward acetaldehyde for Ag/OMS-2-CP catalyst calcined at 400 and 500 °C (Reaction conditions: m = 0.1 g, GHSV = 36,000 ml g<sup>-1</sup> H<sup>-1</sup>, Et/O<sub>2</sub> = 1/9).

(>95%) and high conversion (~53% for Ag-containing samples) at temperatures below 170 °C. However, elevation of reaction temperature results in increased total oxidation activity, and selectivity toward acetaldehyde decreases sharply. Catalytic activity of the crystalline Ag-containing samples normalized on the catalyst mass is higher than that for the OMS-2 (Table 3). Increased reaction rates for Ag-containing catalysts may be explained by increased reaction ability of surface oxygen in the presence of silver, which is confirmed by the TPR-H<sub>2</sub> data (Fig. 6a). Fig. 10 shows the influence of the calcination temperature on the activity of the Ag/OMS-2-CP sample calcined at 400 and 500 °C. One can see that activity and selectivity are similar for both samples due to localization of the Mn<sub>2</sub>O<sub>3</sub> phase not on the surface, but inside the OMS-2 crystallites.

Temperature dependences of ethanol conversion and selectivity toward acetaldehyde and CO<sub>x</sub> are shown in Fig. 11 (a–c) for supported OMS-2 catalysts and the Ag/SiO<sub>2</sub> sample. It is clearly seen that the activity of the Ag-containing catalysts is higher than that of the OMS-2/SiO<sub>2</sub> sample, which correlates with improving of redox properties of the catalysts (Fig. 6b, Fig. 7b). Reduction temperature of manganese oxides decreases, and reoxidation rate increases in the presence of silver in the catalyst composition. The activities of the Ag/SiO<sub>2</sub> and Ag/OMS-2/SiO<sub>2</sub>-Cl samples are similar. However, the Mn-containing sample is characterized by lower selectivity at temperatures above 220 °C. Thus, the active species participating in selective ethanol oxidation are silver sites for both catalysts. Increased CO<sub>2</sub> yield above 220 °C for Mn-containing samples is

connected with total oxidation of ethanol on the Ag-MnO<sub>x</sub> interfacial sites as well as on the MnO<sub>x</sub> sites. The amount of silver in the Ag/OMS-2/SiO<sub>2</sub>-CP catalyst is only 0.95 wt%. However, the activity of this catalyst in the temperature range from 130 to 180 °C is slightly higher than for those for the Ag/OMS-2/SiO<sub>2</sub>-Cl and Ag/SiO<sub>2</sub> samples containing 5 wt% of silver. Formation of oxygen vacancies due to introduction of silver into the manganese oxide structure and the appearance of Ag-MnO<sub>x</sub> sites may play a crucial role in ethanol oxidation.

It is noteworthy that ethanol oxidation over supported OMS-2/SiO<sub>2</sub>, Ag/OMS-2/SiO<sub>2</sub>-Cl, and Ag/OMS-2/SiO<sub>2</sub>-CP catalysts can be carried out at higher temperatures than over the crystalline catalysts while maintaining high selectivity toward acetaldehyde. Selectivity of 93–98% and conversion of ~72 and 50% can be achieved at 200 °C for Ag-containing samples and the OMS-2/SiO<sub>2</sub>, respectively. Fig. 12 shows the stability test with 0.1 g of catalyst for the crystalline Ag/OMS-2-CP and supported Ag/OMS-2/SiO<sub>2</sub>-CP samples. One can see that both catalysts give stable conversion and selectivity toward acetaldehyde for at least 5 h. The supported catalyst gives ~65% ethanol conversion and ~85% selectivity toward acetaldehyde at 230 °C, while the crystalline sample gives 48% conversion and only ~58% selectivity to acetaldehyde at 200 °C. Thus, the use of silica support for crystalline Ag/OMS-2 composites allows controlling the catalytic properties in ethanol oxidation and significantly improving the selectivity toward acetaldehyde under selected conditions and an ethanol/O<sub>2</sub> ratio of 1/9.

Comparison of the activity and selectivity toward acetaldehyde for the prepared catalysts with the literature is shown in Table 3. One of the main parameters, which significantly affects the selectivity toward acetaldehyde, is the ethanol/O<sub>2</sub> molar ratio in the feed flow [45]. In the literature, the silver-containing catalysts are commonly tested in the gas mixture with an ethanol/O<sub>2</sub> molar ratio ranging from 0.33 to 2 [60–62]. In industry, air is used as an oxidant. This allows diluting the feed flow with N<sub>2</sub> and increasing productivity of the process. The increase in oxygen content in the reactant flow is accompanied by sharp growth of the yields of byproducts such as acetic acid, ethyl acetate, and CO<sub>x</sub>. The main advantage of our supported catalysts is an operation in oxygen-rich gas mixtures while maintaining high selectivity toward acetaldehyde. Thus, our supported OMS-2 catalysts have comparable and higher space-time yield (STY) of acetaldehyde in comparison with known silver catalysts. Moreover, the main by-product of the reaction is CO<sub>2</sub>. Therefore, acetaldehyde may be easily separated from the reaction mixture.

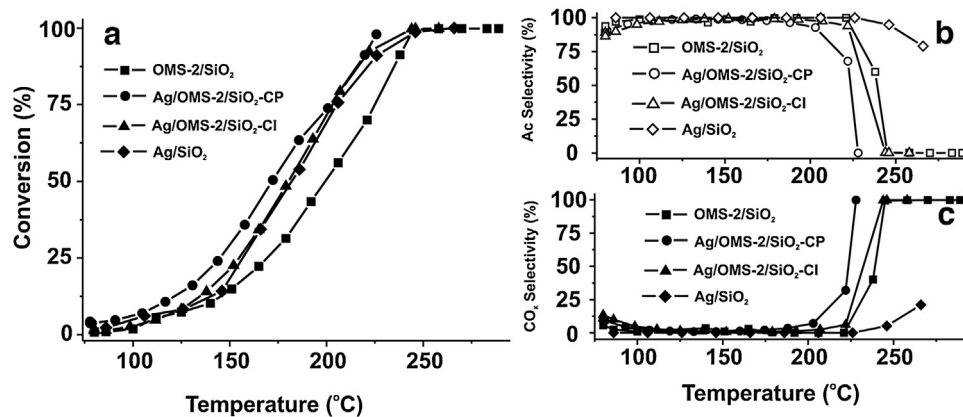


**Fig. 11.** Temperature dependences of ethanol conversion (a) and selectivity toward acetaldehyde (b) and CO<sub>x</sub> (c) for supported OMS-2 catalysts and Ag/SiO<sub>2</sub> sample (Reaction conditions: m = 0.5 g, GHSV = 7200 ml g<sup>-1</sup> H<sup>-1</sup>, Et/O<sub>2</sub> = 1/9).

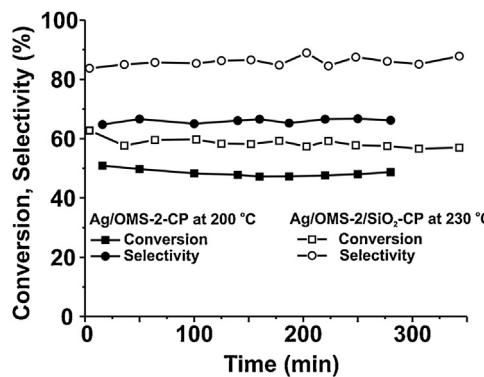


**Fig. 12.** Stability test of the crystalline Ag/OMS-2-CP and supported Ag/OMS-2-CP/SiO<sub>2</sub>-CP samples for ethanol oxidation (Reaction conditions: m = 0.1 g, GHSV = 36,000 ml g<sup>-1</sup> H<sup>-1</sup>, Et/O<sub>2</sub> = 1/9).

#### 4. Conclusion

Crystalline and silica-supported OMS-2 catalysts with and without the addition of Ag were prepared using co-precipitation, impregnation, and consecutive impregnation techniques and tested in the gas-phase selective oxidation of ethanol to acetaldehyde. Investigation of the catalysts by physical-chemical methods showed that the preparation method influenced the localization of silver for both the crystalline and supported catalysts. Consequently, the samples had different active sites. Co-precipitation provided the introduction of silver ions into the OMS-2 framework, while impregnation and consecutive impregnation resulted in localization of silver species on the external surface of the OMS-2 or silica supports. Interaction of silver species with manganese dioxide improved both the reducing and reoxidation abilities of the samples, resulting in higher activity of the silver-containing catalysts. However, the selectivity to acetaldehyde sharply decreased with increased reaction temperature due to the total oxidation process. Increased CO<sub>2</sub> yield for the supported Mn-containing composites compared to the Ag/SiO<sub>2</sub> sample was connected with total oxidation of ethanol on the Ag-MnO<sub>x</sub> sites and also on MnO<sub>x</sub> sites. On the other hand, formation of Ag-MnO<sub>x</sub> sites in the supported catalysts by introducing of silver ions into the channels of the OMS-2 was favorable for the oxidation rate, while formation of Ag/MnO<sub>x</sub> interfaces did not improve conversion of ethanol compared to the Ag/SiO<sub>2</sub> catalyst. The use of silica support for the Ag/OMS-2 composites allowed improving the selectivity toward acetaldehyde in an extended temperature range and, therefore, increasing the yield of acetaldehyde in comparison with the crystalline samples. More-

over, the oxidation process could be carried out in an oxygen-rich mixture with high selectivity toward acetaldehyde and only CO<sub>2</sub> be formed as a byproduct.

#### Acknowledgments

This work was supported by “The Tomsk State University Academic D.I. Mendeleev Fund Program” grant (8.2.07.2015) in 2015–2016. The authors thank Jean Kollantai, Tomsk State University, for style review.

#### References

- [1] A. Corma, S. Iborra, A. Velty, Chem. Rev. 107 (2007) 2411–2502.
- [2] J.V. Ochoa, F. Cavani, RSC Green Chem. 28 (2015) 203–230.
- [3] V.I. Sobolev, K.Yu. Koltunov, ChemCatChem 3 (2011) 1143–1145.
- [4] O.V. Vodyankina, A.S. Blokhina, I.A. Kurzina, V.I. Sobolev, K.Yu. Koltunov, L.N. Chukhlomina, E.S. Dvilius, Catal. Today 203 (2013) 127–132.
- [5] A.S. Blokhina, I.A. Kurzina, V.I. Sobolev, K.Yu. Koltunov, G.V. Mamontov, O.V. Vodyankina, Kinet. Catal. 53 (2012) 477–481.
- [6] C. Junli, L. Juan, L. Qiyng, H. Xiumin, S. Wenjie, Chin. J. Catal. 28 (12) (2007) 1034–1036.
- [7] G.D. Yadav, R.K. Mewada, Chem. Eng. Res. Des. 90 (2012) 86–97.
- [8] H. Zhou, J.Y. Wang, X. Chen, Microporous Mesoporous Mat. 21 (1998) 315–324.
- [9] N.N. Opembe, C. Guild, C. King'ondu, N.C. Nelson, I.I. Slowing, S.L. Suib, Indian Eng. Chem. Res. 53 (2014) 19044–19051.
- [10] G.D. Yadav, A.R. Yadav, J. Mol. Catal. A: Chem. 380 (2013) 70–77.
- [11] V.D. Makwana, L.J. Garces, J. Liu, Catal. Today 85 (2003) 225–233.
- [12] D.A. Tompsett, S.C. Parker, M.S. Islam, J. Mater. Chem. A 2 (2014) 15509–15518.
- [13] S. Navaladan, V. Balasubramanian, K.V. Thirukkallam, RSC Adv. 4 (2014) 33911–33922.
- [14] P.H. Ho, S.C. Lee, J. Kim, D. Lee, H.C. Woo, Fuel Process. Technol. 131 (2015) 238–246.
- [15] P.H. Ho, S.C. Lee, J. Kim, D. Lee, H.C. Woo, Korean J. Chem. Eng. 32 (9) (2015) 1766–1773.
- [16] M. Prabu, K. Ramalingam, RSC Adv. 5 (2015) 18554–18564.
- [17] L. Li, E. Cockayne, I. Williamson, L. Espinal, W. Wong-Ng, Chem. Phys. Lett. 580 (2013) 120–125.
- [18] X. Meng, C. Yu, G. Chen, P. Zhao, Cat. Sci. Technol. 5 (2015) 372–379.
- [19] K. Yamaguchi, K. Sakagami, Y. Miyamoto, X. Jin, N. Mizuno, Org. Biomol. Chem. 12 (2014) 9200–9206.
- [20] X. Meng, J. Zhang, G. Chen, B. Chen, P. Zhao, Catal. Commun. 69 (2015) 239–242.
- [21] X. Yang, C. Yin, J. Han, Y. Wu, React. Kinet. Mech. Catal. 117 (2016) 269–281.
- [22] M. Ousmane, G. Perrussel, Z. Yan, J.-M. Clacens, F. De Campo, M. Pera-Titus, J. Catal. 309 (2014) 439–452.
- [23] H. Zhou, J.Y. Wang, X. Chen, Microporous Mesoporous Mat. 21 (1998) 315–324.
- [24] V. Mahdavi, S. Soleimani, Mater. Res. Bull. 51 (2014) 153–160.
- [25] L. Duan, B. Sun, M. Wei, S. Luo, F. Pan, A. Xu, X. Li, J. Hazard. Mater. 285 (2015) 356–365.
- [26] S. Luo, L. Duan, B. Sun, M. Wei, X. Li, A. Xu, Appl. Catal. B: Environ. 164 (2015) 92–99.
- [27] G. Qiu, H. Huang, S. Dharmarathna, E. Benbow, L. Stafford, S.L. Suib, Chem. Mater. 23 (2011) 3892–3901.

- [28] G.G. Xia, Y.G. Yin, W.S. Willis, J.Y. Wang, S.L. Suib, *J. Catal.* 185 (1999) 91–105.
- [29] J. Liu, V. Makwana, J. Cai, S.L. Suib, *J. Phys. Chem. B* 107 (2003) 9185–9194.
- [30] V.P. Santos, M.F.R. Pereira, *Appl. Catal. B: Environ.* 99 (2010) 353–363.
- [31] R. Kumar, S. Sithambaram, S.L. Suib, *J. Catal.* 262 (2009) 304–313.
- [32] R. Ghosh, X. Shen, J.C. Villegas, *J. Phys. Chem. B* 110 (2006) 7592–7599.
- [33] H. Tian, J. He, L. Liu, *Ceram. Int.* 39 (2013) 315–321.
- [34] C. Almquist, M. Krekeler, L. Jiang, *Chem. Eng. J.* 252 (2014) 249–262.
- [35] Y.F. Shen, R.P. Zerger, R.N. DeGuzman, S.L. Suib, L. McCurdy, D.I. Potter, C.L. O'Young, *Science* 260 (1993) 511–515.
- [36] V.D. Makwana, Y.C. Son, A.R. Howel, *J. Catal.* 210 (2002) 46–52.
- [37] W. Zhong, S.R. Kirk, D. Yin, Y. Li, R. Zou, L. Mao, G. Zou, *Chem. Eng. J.* 280 (2015) 737–747.
- [38] V. Mahdavi, M. Mardani, *Mater. Chem. Phys.* 155 (2015) 136–146.
- [39] J.M. Zamaro, A.V. Boix, A. Martinez-Hernandez, *Catal. Commun.* 69 (2015) 212–216.
- [40] H. Yang, J. Deng, S. Xie, Y. Jiang, H. Dai, C.T. Au, *Appl. Catal. A: Gen.* 507 (2015) 139–148.
- [41] M.A. Peluso, E. Pronsato, J.E. Sambeth, H.J. Thomas, G. Busca, *Appl. Catal. B: Environ.* 78 (2008) 73–79.
- [42] H. Perez, P. Navarro, G. Torres, O. Sanz, M. Montes, *Catal. Today* 212 (2013) 149–156.
- [43] H. Sun, Z. Liu, S. Chen, X. Quan, *Chem. Eng. J.* 270 (2015) 58–65.
- [44] Y. Yang, J. Huang, S. Zhang, *Appl. Catal. B: Environ.* 150–151 (2014) 167–178.
- [45] O.V. Vodyankina, A.S. Blokhina, I.A. Kurzina, V.I. Sobolev, K.Yu. Koltunov, L.N. Chukhlomina, E.S. Dvilis, *Catal. Today* 203 (2013) 127–132.
- [46] R. Hu, L. Xie, S. Ding, J. Hou, Y. Cheng, D. Wang, *Catal. Today* 131 (2008) 513–519.
- [47] M.F.L. Haris, C.-Y. Yin, Z.-T. Jiang, B.-M. Goh, X. Chen, W.A. Al-Masry, A.M. Abukhalaf, M. El-Harbawi, N.M. Huang, H.N. Lim, *Ceram. Int.* 40 (2013) 1245–1250.
- [48] R.N. DeGuzman, Y.-F. Shen, E.J. Neth, S.L. Suib, C.-L. O'Young, S. Levine, J.M. Newsam, *Chem. Mater.* 6 (1994) 815–821.
- [49] M. Özcar, A.S. Poyraz, H.C. Genuino, C.-H. Kuo, Y. Meng, S.L. Suib, *Appl. Catal. A: Gen.* 463–463 (2013) 64–74.
- [50] L. Wu, F. Xu, Y. Zhu, A.B. Brady, J. Huang, J.L. Durham, E. Dooryhee, A.C. Marschilok, E.S. Takeuchi, K.J. Takeuchi, *ACS Nano* 9 (2015) 8430–8439.
- [51] Z. Qu, Y. Bu, Y. Qin, Y. Wang, Q. Fu, *Appl. Cat. B: Environ.* 132–133 (2013) 353–362.
- [52] X. Zhang, Z. Qu, X. Li, M. Wen, X. Quan, D. Ma, J. Wu, *Sep. Purif. Technol.* 72 (2010) 395–400.
- [53] A.R. Gandhe, J.S. Rebello, J.L. Figueiredo, *Appl. Catal. B: Environ.* 72 (2007) 129–135.
- [54] R. Hu, C. Yan, L. Xie, *Int. J. Hydrogen Energy* 36 (2011) 64–71.
- [55] R. Xu, X. Wang, D. Wang, K. Zhou, Y. Li, *J. Catal.* 237 (2006) 426–430.
- [56] M. Bowker, M.A. Barreau, R.J. Madix, *Surf. Sci.* 92 (1980) 528–548.
- [57] G.V. Mamontov, O.V. Magaev, A.S. Knyazev, O.V. Vodyankina, *Catal. Today* 203 (2013) 122–126.
- [58] G.V. Mamontov, V.V. Dutov, V.I. Sobolev, O.V. Vodyankina, *Kinet. Catal.* 54 (2013) 487–491.
- [59] A.S. Savel'eva, O.V. Vodyankina, *Rus. J. Phys. Chem. A* 88 (2014) 2203–2208.
- [60] Z. Li, J. Xu, X. Gu, K. Wang, W. Wang, X. Zhang, Z. Zhang, Y. Ding, *Chem. Cat. Chem.* 5 (2013) 1705–1708.
- [61] P. Liu, X. Zhu, S. Yang, T. Li, E.J.M. Hensen, *J. Catal.* 331 (2015) 138–146.
- [62] J. Chen, X. Tang, J. Liu, E. Zhan, J. Li, X. Huang, W. Shen, *Chem. Mater.* 19 (2007) 4292–4299.